Journal of Catalysis 265 (2009) 170–180

Contents lists available at ScienceDirect

Journal of Catalysis

journal homepage: www.elsevier.com/locate/jcat

Desilication of ferrierite zeolite for porosity generation and improved effectiveness in polyethylene pyrolysis

Adriana Bonilla [a], David Baudouin [a], Javier Pérez-Ramírez [a,b,*]

[a] Institute of Chemical Research of Catalonia (ICIQ), Avinguda Països Catalans 16, 43007 Tarragona, Spain
[b] Catalan Institution for Research and Advanced Studies (ICREA), Passeig Lluís Companys 23, 08010 Barcelona, Spain

ARTICLE INFO

Article history:
Received 6 January 2009
Revised 23 April 2009
Accepted 27 April 2009
Available online 20 May 2009

Keywords:
Ferrierite
Hierarchical zeolites
Desilication
Mesoporosity
Accessibility
Pyrolysis
LDPE degradation

ABSTRACT

Desilication of the medium-pore ferrierite zeolite in sodium hydroxide solutions was conducted to modify the porous structure and to create structural defects, resulting in enhanced accessibility and ultimately improved catalytic performance. Commercial H-ferrierite (Si/Al = 29) with the characteristic plate-like morphology was used as starting material. The attack by NaOH induces deaggregation, exfoliation, fracture, and ultimately perforation of the ferrierite crystals, resulting in mesoporosity of combined inter- and intracrystalline nature. The parent and treated samples were characterized by ICP-OES, XRD, N_2 adsorption, SEM, TEM, ^{27}Al and ^{29}Si MAS-NMR, FTIR, and NH_3-TPD. Optimization of the treatment conditions (NaOH concentration, temperature, and time) is required to introduce substantial mesoporosity without significantly altering the micropore structure due to excessive Si leaching. Compared to other frameworks (e.g. MFI, MTW, MOR, and BEA), FER requires harsher conditions to extract silicon leading to mesoporosity. Under optimal conditions, the mesopore surface area of the NaOH-treated ferrierite increased by a factor of 3–4 with respect to the parent zeolite, while mostly preserving the native crystallinity and acidity. The ability of NaOH to induce porosity changes in FER largely exceeds conventional dealumination post-treatments. The benefit of the introduced porosity was demonstrated in the catalytic pyrolysis of low-density polyethylene.

1. Introduction

The unique properties of zeolites, viz. crystallinity, high-surface area, acidity, ion-exchange capacity, and shape-selective character, make them hegemonic materials in many industrial applications related to catalysis, adsorption, and separation. The sole presence of micropores (0.25–1 nm) in zeolite frameworks often imposes diffusion limitations due to hindered access and slow intracrystalline transport of reactants and products to and from the bulk of the crystal [1–4]. Diffusion limitations result in a poor utilization of the zeolite volume in catalyzed reactions, limiting the activity and occasionally also the selectivity and lifetime.

Ferrierite (FER topology) is a medium-pore zeolite that is produced commercially, and it displays remarkable catalytic performance, as such or modified, in a variety of acid and redox reactions: skeletal isomerization of n-alkenes to iso-alkenes [5–8], n-paraffin cracking [9,10], dewaxing of lube oil base stocks and middle distillates by selectively hydrocracking long-chain paraffins [11], alkane hydroisomerization [12], isomerization of m-xylene [13], α-pinene [14], and dichlorobenzenes [15], isobutene trimerization [16], methanol to olefins [17], styrene epoxidation [18], propane oxidative dehydrogenation [19], NO_x reduction [20,21], and N_2O decomposition [22]. The ferrierite structure comprises an orthorhombic framework containing the main 10-MR channels (0.42 × 0.54 nm) in the [001] direction interconnected with side 8-MR channels (0.35 × 0.48 nm) in the [010] direction (Fig. 1). The intersection of the 8-MR channels and the 6-MR channels in the c-direction leads to spherical cavities (FER cage) [23,24].

Ferrierite is amenable to industrial application owing to its excellent stability toward (hydro)thermal and chemical treatments [25]. However, the reduced dimension of the pore system in relation to the size of typical substrates can be a restrictive factor to fully exploit its potential in some of the above reactions as well as to expand its application to new processes. For example, van Well et al. [26] reported that ferrierite operates as a one-dimensional pore system for long-chain molecules (C5+) and that pore blockage by coke formation results in a large inhibiting effect. In situ infrared studies by Meunier et al. [6] concluded that the n-butene isomerization was effectively limited to the acid sites located near the surface of the H-ferrierite crystals (pore mouth catalysis), while the bulk of the crystals are filled with slowly diffusing species such as branched C8 hydrocarbons and aromatics.

Diffusion limitations in zeolites can be alleviated by enlarging the micropore size or by shortening the diffusion length [4].

* Corresponding author. Fax: +34 977 920 224.
E-mail address: jperez@iciq.es (J. Pérez-Ramírez).

0021-9517/$ - see front matter © 2009 Elsevier Inc. All rights reserved.
doi:10.1016/j.jcat.2009.04.022

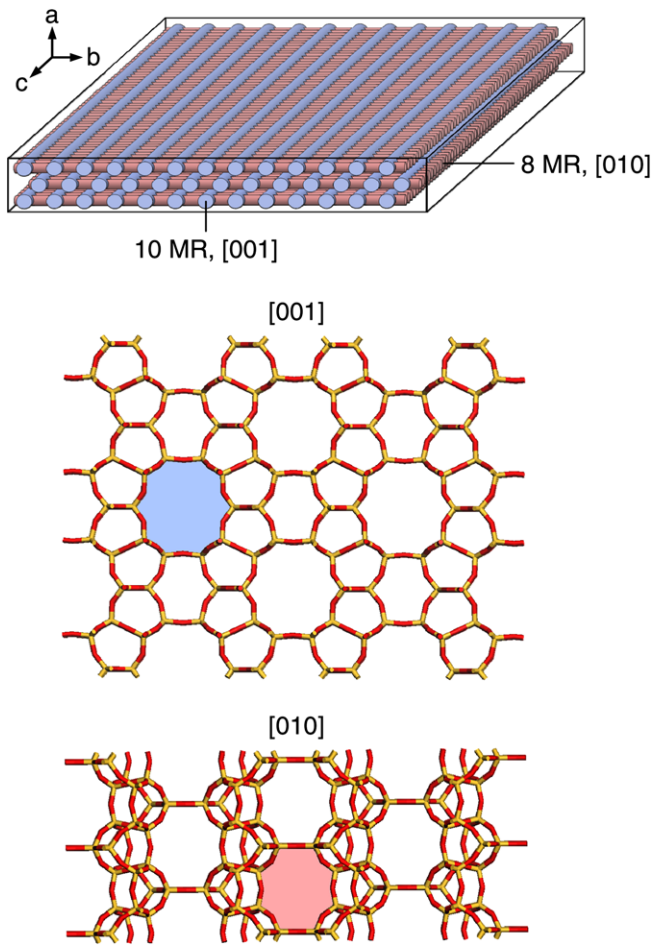

Fig. 1. Structure of ferrierite in the [001] and [010] directions. The openings of the 10-MR and 8-MR pores are colored.

Strategies for the latter purpose comprise the preparation of delaminated zeolites [27], zeolite nanocrystals [28], composites of zeolites and ordered mesoporous materials [29], and mesoporous zeolite crystals [30]. To date, the only demonstrated way to enhance the accessibility of ferrierite consists in delaminating the lamellar PREFER precursor [31]. This treatment leads to ITQ-6, a nanosheet-based non-microporous material with an external surface area of 600 $m^2\,g^{-1}$. This route requires a less conventional template to synthesize PREFER (4-amino-2,2,6,6-tetramethylpiperidine) and an ionic surfactant (cetyltrimethylammonium bromide) as a swelling agent. In consideration of wide implementation, the use of commercially available ferrierite and cheap reagents is highly desirable. Unfortunately, post-synthesis dealumination by high-temperature calcination, steaming, treatment with HCl, oxalic acid, $(NH_4)_2SiF_6$, or $SiCl_4$ causes no modification of the porous characteristics of ferrierite [8,13,32,33] in contrast to the noticeable effect on other zeolite structures [34].

The selective extraction of framework silicon in aqueous NaOH solutions, known as desilication, is a versatile, effective, and simple approach to generate intracrystalline mesoporosity in ZSM-5 [35,36], ZSM-12 [37], mordenite [38], and beta [39,40] zeolites. As a result, a hierarchical zeolite is obtained, combining the unique catalytic properties of the intrinsic micropores and the facilitated access and improved transport consequence of a complementary mesopore network. Desilication also proved to be suitable to prepare uniform octadecasil nanocrystals with a high external surface area [41]. Preliminary work by some of us [42] showed that ferrierite was also susceptible to extensive mesopore formation by alkaline treatment under relatively harsh conditions (0.5 M NaOH, 348 K, 5 h). However, the increase in mesopore surface area (from 20 to 130 $m^2\,g^{-1}$) was accompanied by a marked decrease in micropore volume (from 0.13 to 0.08 $cm^3\,g^{-1}$) due to the excessive silicon leaching. Accordingly, optimization of the alkaline treatment is required to develop significant mesoporosity while preserving to the largest possible extent the crystallinity and acidity of the original microporous material.

Herein, we have subjected a commercial ferrierite sample (Si/Al = 29) to NaOH treatments in order to generate controlled mesoporosity by selective silicon extraction. The bulk Si/Al ratio of the starting material was the optimal window of 25–50 [43]. The influence of the NaOH concentration, temperature, and time on the porous properties was screened and compared with conventional dealumination post-treatments (steam and acid leaching). Based on detailed characterization, insights into the desilication mechanism and the nature of the introduced porosity are discussed. The catalytic performance of the ferrierite samples was evaluated in the pyrolysis of low-density polyethylene. This application is of practical importance for chemical recycling of plastic waste by transformation into valuable fuels or chemicals [44]. In this classical cracking reaction, purely microporous ferrierite displays a low degradation activity compared to other zeolite types such as beta and ZSM-5 [45]. This was attributed to mass-transfer constraints of the branched polymer to penetrate the relatively small ferrierite micropores. Therefore, it is a suitable model reaction to evaluate the eventual benefit of the introduced secondary mesoporosity on the catalytic performance.

2. Experimental

2.1. Parent zeolite and treatments

A commercial ferrierite from Zeolyst (CP 914, nominal Si/Al = 27, NH_4-form) was used as starting material. The sodium content was <0.004 wt.%. Prior to the characterization and treatments, the as-received sample was calcined in static air at 823 K for 5 h using a heating rate of 5 K min^{-1}. The resulting sample is referred to as the parent zeolite (P).

Alkaline treatments (ATs) of the zeolite were carried out in a 16-parallel reactor system (MultiMax from Mettler Toledo), varying NaOH concentration (0.1–1 M), temperature (333–363 K), and time (0.5–9 h). The reactors (17 mm i.d., total volume 50 cm^3) were filled with 10 cm^3 of NaOH aqueous solution, sealed, and introduced in the reactor block. Once the desired temperature was reached, zeolite powder (330 mg) was added to each reactor and stirred magnetically at 500 rpm. After the treatment, the zeolite suspension was cooled down in an ice-water mixture and filtered. The resulting solids were washed with distilled water until pH neutral and dried at 333 K for 12 h. The filtrates were kept for chemical analysis. Finally, the alkaline-treated samples were brought into the protonic form via three successive exchanges in a 0.1 M NH_4NO_3 aqueous solution at room temperature followed by calcination at 823 K for 5 h.

The parent ferrierite was also treated in steam and acid. Steaming (ST) was carried out using a quartz reactor with a shallow bed of zeolite powder (266 mbar H_2O and 40 cm^3 STP min^{-1} of He flow, 150 mg of zeolite, 873 K, 2.5 h). Treatments in hydrochloric acid (HCl) and oxalic acid (OA) were carried out at the following conditions: (i) 10 cm^3 of 5.25 M HCl aqueous solution, 330 mg of zeolite, 298 K, 4 h and (ii) 10 cm^3 of 0.5 M $H_2C_2O_4$ aqueous solution, 500 mg of zeolite, 343 K, 2 h. The resulting samples were filtered, washed, dried at 333 K, and calcined at 823 K for 5 h.

Table 1
Textural properties of the parent and treated ferrierite samples.

Sample[a]	C (M)	T (K)	t (h)	V_{pore} ($cm^3\ g^{-1}$)	V_{micro}[b] ($cm^3\ g^{-1}$)	S_{meso}[b] ($m^2\ g^{-1}$)	S_{BET}[c] ($m^2\ g^{-1}$)
P	–	–	–	0.22	0.14	20	369
AT-1	0.2	333	0.5	0.21	0.13	19	342
AT-2	0.2	333	1	0.23	0.13	33	339
AT-3	0.2	333	2	0.25	0.12	58	343
AT-4	0.2	333	10	0.23	0.13	36	346
AT-5	1	333	0.5	0.29	0.11	55	320
AT-6	0.2	343	0.5	0.21	0.12	20	326
AT-7	0.2	353	0.5	0.22	0.12	30	323
AT-8	0.1	353	3	0.22	0.13	16	336
AT-9	0.2	353	3	0.25	0.12	49	300
AT-10	0.35	353	3	0.31	0.10	77	337
AT-11	0.5	353	3	0.36	0.08	107	304
AT-12	0.75	353	3	0.28	0.04	80	174
AT-13	1	353	3	0.29	0.01	56	67
AT-14	0.2	343	3	0.21	0.13	22	335
AT-15	0.2	363	3	0.31	0.13	70	383
AT-16	0.2	353	9	0.35	0.12	93	376
HCl	5.25	298	4	0.22	0.13	22	334
ST	266[d]	873	2.5	0.22	0.12	29	324
ST-AT-15	0.2	363	3	0.26	0.13	50	375
OA	0.5	343	2	0.22	0.14	18	369
OA-AT-15	0.2	363	3	0.30	0.13	71	385

[a] P: parent zeolite; AT: alkaline treatment in sodium hydroxide; HCl: treatment in hydrochloric acid; ST: steam treatment; OA: treatment in oxalic acid. Sample ST-AT-15 (OA-AT-15) was obtained by steam (oxalic acid) treatment of the parent zeolite followed by NaOH treatment at AT-15 conditions.
[b] t-Plot method.
[c] BET method.
[d] Partial steam pressure in mbar.

Table 1 collects all the samples prepared in this study and the specific treatment conditions. The notation used throughout the manuscript is explained in the footnote of the table.

2.2. Characterization

Si and Al concentrations in the solids and in the filtrates obtained by alkaline treatment were determined by Inductively Coupled Plasma-Optical Emission Spectroscopy (ICP-OES) (Perkin–Elmer Optima 3200RL).

X-ray diffraction (XRD) patterns were measured in a Siemens D5000 diffractometer with Bragg-Brentano geometry and Ni-filtered Cu Kα radiation (λ = 0.1541 nm). Data were recorded in the range 5–50° 2θ with an angular step size of 0.05° and a counting time of 8 s per step.

Scanning electron microscopy (SEM) was carried out in a JEOL JSM-6400 microscope operated at 20 kV. The samples were coated with gold.

Transmission electron microscopy (TEM) was carried out in a JEOL JEM-1011 microscope operated at 100 kV and equipped with a SIS Megaview III CCD camera. A few droplets of the sample suspended in ethanol were placed on a carbon-coated copper grid followed by evaporation at ambient conditions.

Nitrogen isotherms at 77 K were measured in a Quantachrome Quadrasorb-SI gas adsorption analyzer. Before the measurement, the samples were degassed in vacuum at 573 K for 10 h. The BET method [46] was applied to calculate the total surface area, which is used for comparative purposes. The t-plot method [47] was used to discriminate between micro- and mesoporosity. The mesopore size distribution was obtained by the BJH model [48] applied to the adsorption branch of the isotherm.

Solid-state magic-angle spinning nuclear magnetic resonance (MAS-NMR) spectra were recorded at a spinning speed of 12 kHz on a Bruker 400 MHz Avance wide-bore spectrometer equipped with a 4 mm BB/1 H probe and 4 mm ZrO_2 rotors. ^{29}Si spectra were recorded using 2000 accumulations at 4.5 μs pulses, an angle of 30°, and a relaxing time of 5 s. ^{27}Al spectra were recorded using 1160 accumulations at 4 μs pulses, an angle of 90°, and a relaxing time of 10 s. DSS (2,2-dimethyl-2-silapentane-5-sulfonic acid) and $NH_4SO_4Al{\cdot}12\ H_2O$ were used as references for silicon and aluminum, respectively.

Fourier transform infrared spectroscopy was recorded in nitrogen at 473 K on a Thermo Nicolet 5700 spectrometer using a SpectraTech Collector II diffuse reflectance (DRIFT) accessory equipped with a high-temperature cell. Prior to the analysis, the sample was dried at 723 K in a flow of N_2 (100 cm^3 STP min^{-1}) for 30 min. Spectra were recorded in the range 650–4000 cm^{-1} with a nominal resolution of 4 cm^{-1} and co-addition of 32 scans.

Temperature-programmed desorption of ammonia (NH_3-TPD) was carried out in a Thermo TPDRO 1100 unit equipped with a thermal conductivity detector. The zeolite (50 mg) was pretreated at 823 K in He flow (20 cm^3 STP min^{-1}) for 2 h. Afterwards, pure NH_3 (25 cm^3 STP min^{-1}) was adsorbed at 473 K for 10 min followed by He purging at the same temperature for 1 h. This procedure was repeated three times. Desorption of NH_3 was monitored in the range 473–973 K using a ramp of 10 K min^{-1}.

2.3. LDPE pyrolysis

The pyrolysis of low-density polyethylene (LDPE, granules, Alfa Aesar) was carried out in a Mettler Toledo TGA/SDTA851e microbalance equipped with a 34-position sample robot. The grounded polymer (3 mg) and the zeolite powder (1 mg, 25% of the total weight) were carefully weighed and intimately mixed in the 70 μl α-Al_2O_3 crucibles of the thermobalance. The pyrolysis was performed in N_2 (70 cm^3 STP min^{-1}) from 298 to 973 K using different heating rates (5, 10, 20, 35, and 50 K min^{-1}). The activation energy (E_a) at different conversion values was determined by the Ozawa method [49] (Eq. (1)), which does not require the previous knowledge of the reaction order. In this equation, β is the heating rate, R is the ideal gas constant, and T is the absolute temperature for the same conversion at each heating rate

$$\frac{d(\log \beta)}{d(1/T)} = -0.4567 \frac{E_a}{R}. \quad (1)$$

3. Results and discussion

3.1. Parent zeolite

The protonic form of ferrierite (denoted P, parent) was obtained by calcination of the as-received zeolite at 823 K. The molar Si/Al ratio in the solid determined by ICP-OES was 29, i.e. very close to the nominal ratio of 27. The sample showed the typical X-ray diffraction pattern of the FER structure (Fig. 2), and consisted of aggregates of plate-like crystals (Fig. 3a and b). These platelets are parallel to the perpendicularly interconnected 8 and 10-MR channels (Fig. 1). The size of the aggregates is rather heterogeneous and goes up to ca. 15 μm as determined by SEM. The single platelets, which can be discerned by transmission electron microscopy (Fig. 4a and b), have a length of 0.3–0.8 μm and a lateral width of 50–150 nm. The N_2 isotherm of the calcined sample is type I (Fig. 5), confirming its microporous character. The textural parameters of this sample are given in Table 1. The micropore volume (V_{micro} = 0.14 $cm^3\ g^{-1}$) is characteristic of ferrierite. The mesopore surface area (S_{meso} = 20 $m^2\ g^{-1}$) results from the crystals' external surface and surface roughness.

3.2. NaOH treatment

3.2.1. Porosity

Table 1 shows the matrix of alkaline treatments (ATs) applied and the impact on the porous properties of the resulting materials. The comparison of P and AT-1 reveals that optimal desilication conditions (0.2 M NaOH, 333 K, 30 min) for other frameworks (MFI, MTW, and MOR) with a similar Si/Al ratio [35–38] did not induce porosity changes in FER. This observation indicates that harsher conditions are required for mesoporosity development in ferrierite by silicon extraction. The higher stability of ferrierite toward desilication in alkaline medium can be related to the higher stability of framework aluminum in this structure, since all T-sites are bonded to five rings [32]. It is known that the presence of the negatively charged AlO_4^- tetrahedral prevents the hydrolysis of the Si–O–Al bond in the presence of OH^- [35]. Accordingly, a direct link should exist between the stability of framework aluminum and its proneness to desilication. This is further substantiated by the facile silicon dissolution of beta in NaOH at mild conditions [39], which correlates with the relative low stability of the framework Al in this structure. The presence of T-sites in four rings of beta, mordenite, ZSM-5, and Y zeolites makes them more susceptible to dealuminate since the tension in smaller rings is larger [32]. In addition to the relative stability and distribution of aluminum, other factors such as the flexibility of the framework and the presence of defect sites might also contribute to the different stabilities of various zeolite types in alkaline conditions.

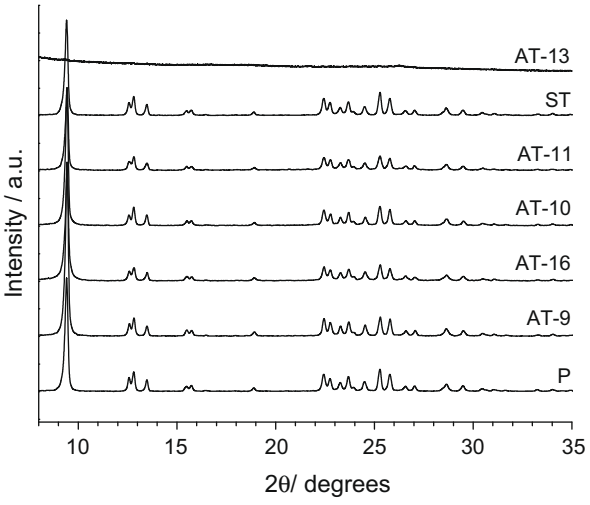

Fig. 2. XRD patterns of the parent and treated ferrierite samples.

An increase in temperature and time increased the S_{meso} of the treated ferrierite, although the most remarkable changes occurred when increasing the NaOH concentration. The dominant factor of the alkali concentration in the desilication process was also concluded for ZSM-12 [37]. The series of samples from AT-9 to AT-13 can be used to represent this effect. As captured in Fig. 6, the S_{meso} goes through a maximum with the NaOH concentration corresponding to AT-11 (107 $m^2\ g^{-1}$ at 0.5 M), while the V_{micro} experiences a progressive decrease. This plot illustrates the required optimization of the desilication treatment for a given zeolite structure in the sense of compromising between the increase in mesopore surface area and the reduction of the intrinsic zeolite microporosity. For example, the gain in S_{meso} of AT-11 is more than 450%, and is accompanied by a V_{micro} loss of 43% with respect to the parent zeolite. Above a certain NaOH concentration, the Si leaching is excessive, provoking the enlargement of the formed mesopores toward the macropore region, thereby causing a decrease in S_{meso}. The same volcano-type dependency of Fig. 6 was obtained with other treatment variables such as time and temperature. For example, the series of samples from AT-1 to AT-4, in which a fixed temperature (333 K) and NaOH concentration (0.2 M) were applied, presents a maximal S_{meso} at 2 h (Table 1). The samples AT-15 (0.2 M, 363 K, 3 h) and AT-16 (0.2 M, 353 K, 9 h) are of particular interest, as the gain in S_{meso} is more than 250% and 350% with respect to the parent zeolite, respectively, while the V_{micro} is decreased to a minor extent (less than 15%). These specimens can be regarded as *optimal*, since the mesopore surface area in the starting material is enhanced by a factor of 3–4 times while the native microporosity is largely preserved.

As shown in Fig. 5, the alkaline-treated samples have combined type I and type IV isotherms, with nitrogen uptakes at low and intermediate relative pressures and the development of a hysteresis loop in the mesopore region. These fingerprints are indicative of hierarchical porous systems that combine micro- and mesoporosity [4]. The N_2 uptake of AT-11 at low p/p_0 is lower than that of the parent zeolite due to the significantly decreased micropore volume at the applied desilication conditions. The alkaline-treated ferrierite samples do not have a defined mesopore size, but instead have a broad distribution of large mesopores (Fig. 5, inset). This differs from other alkaline-treated zeolites (ZSM-5, ZSM-12, mordenite, and beta), in which intracrystalline mesopores centered in the range of 3–10 nm have been typically obtained [35–40]. We put forward that this distinctive feature is connected with the particular morphology of the FER crystals, consisting of very thin platelets (50–150 nm, Fig. 4b). The small thickness of the crystals could cause the absence of a distinct increase in adsorption volume due to condensation in mesopores since the overall mesopore volume is relatively small and, as a consequence, the pore size distribution model (irrespective of which model is used) has difficulties in finding a distinct inflection point. Thus, it cannot be excluded that intracrystalline porosity in the alkaline-treated ferrierite platelets (e.g. as in Fig. 4f, vide infra) is not fully accounted for by the BJH model.

3.2.2. Chemical composition

Mesopore formation in the alkaline-treated zeolites has been related to the preferential framework silicon extraction with re-

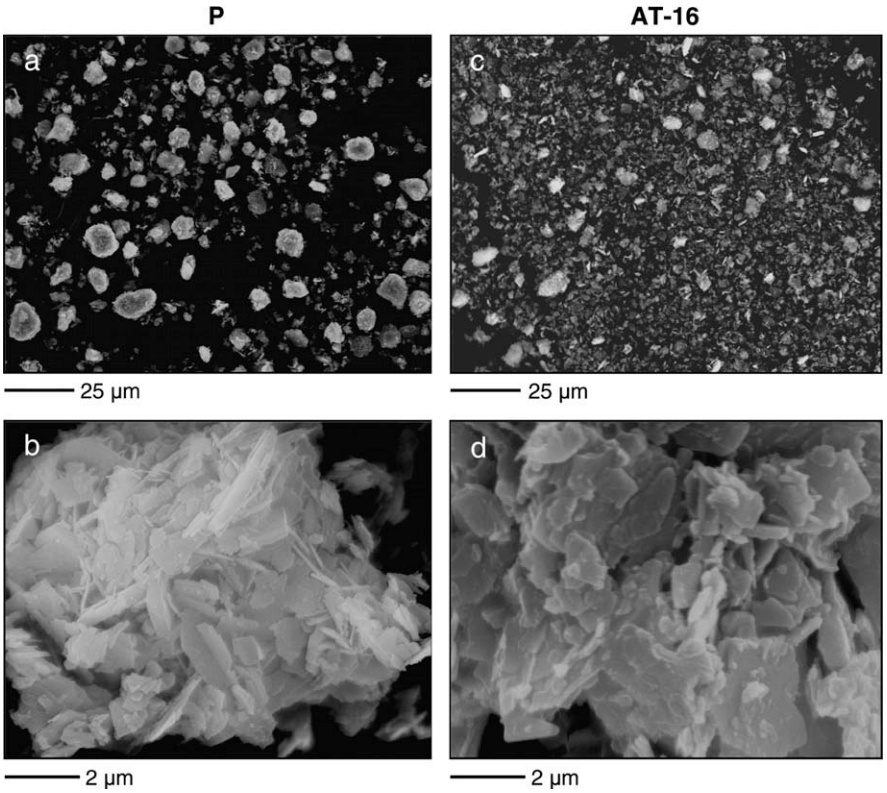

Fig. 3. SEM of the parent and alkaline-treated ferrierite samples.

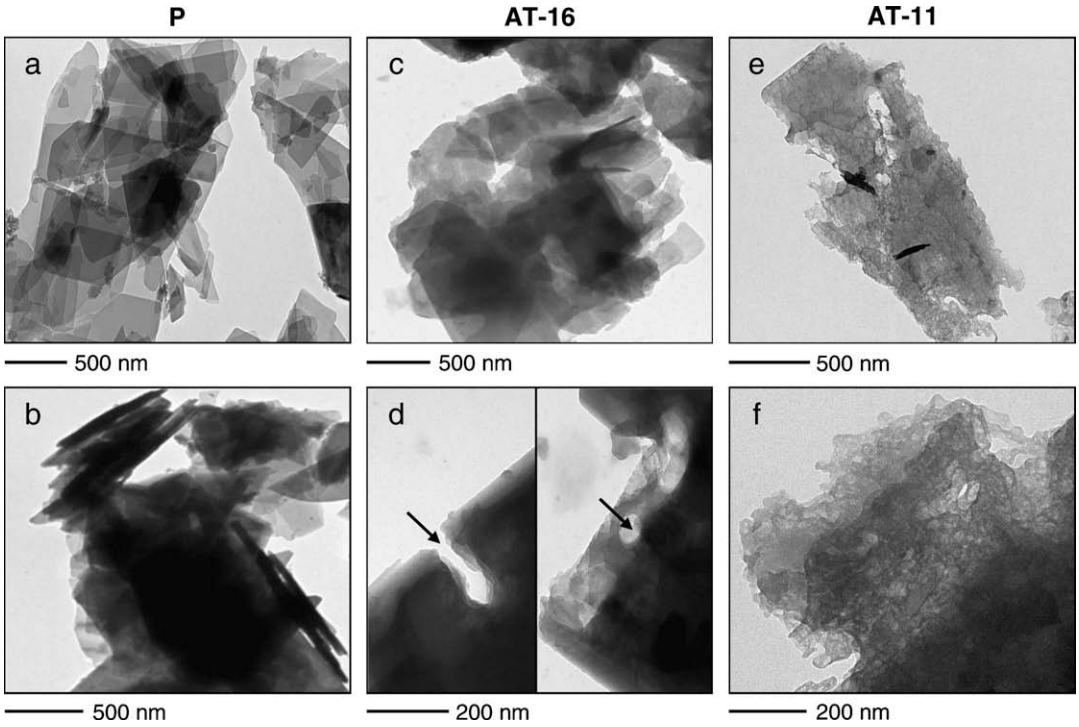

Fig. 4. TEM of the parent ferrierite and alkaline-treated samples.

spect to aluminum [50,51], and hence a decreased Si/Al ratio in the resulting samples can be expected. Table 2 shows the molar Si/Al ratio in the solids and the Si and Al concentration in the filtrates, respectively, determined by ICP-OES. The molar Si/Al ratio decreased from 29 in the parent zeolite to 20 (AT-15) and 17 (AT-16) in the optimal NaOH-treated samples. A clear correlation was obtained between the severity of the alkaline post-treatment, the increased silicon concentration in the filtrates, the decreased Si/Al in the solids, and the increased mesopore surface area. In the filtrates, the Si concentration was 2 orders of magnitude higher

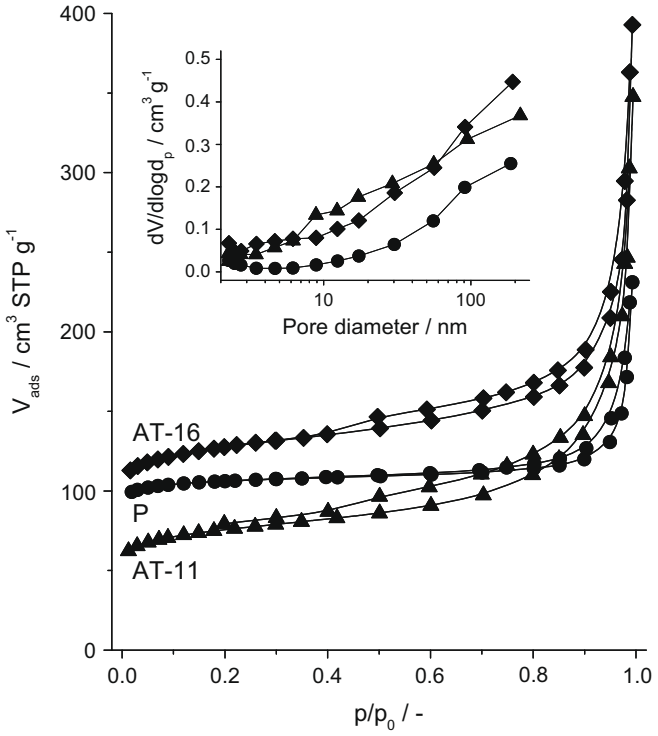

Fig. 5. N_2 isotherms of the parent and alkaline-treated ferrierite samples. Inset: adsorption BJH pore size distributions.

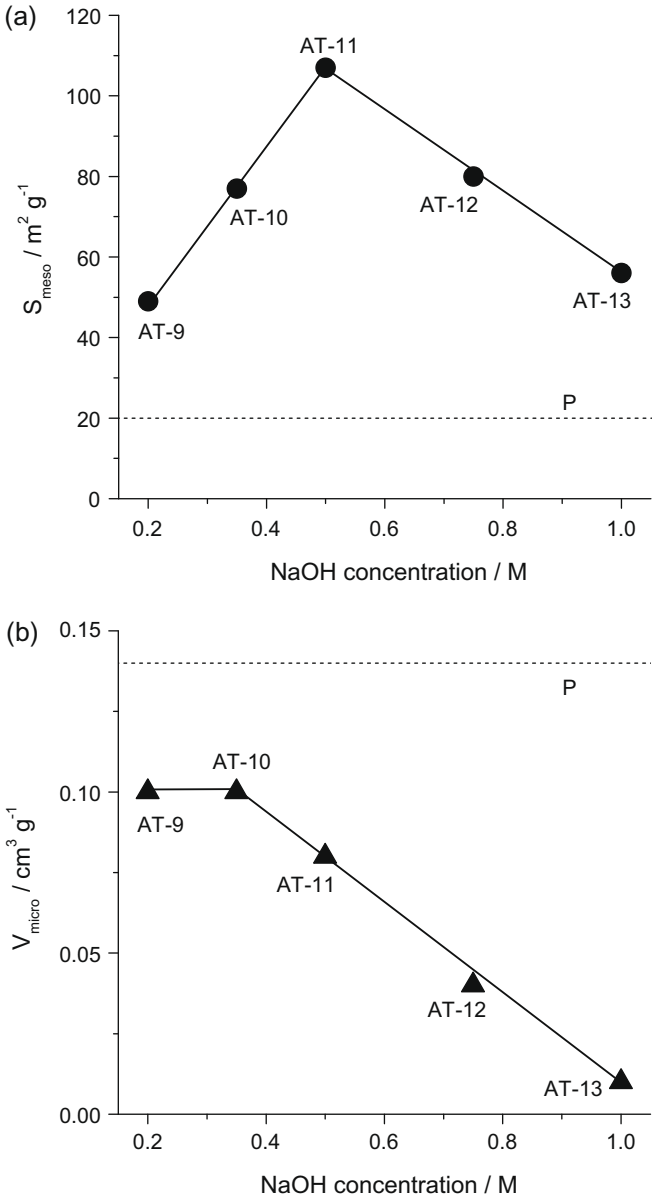

Fig. 6. (a) Mesopore surface area and (b) micropore volume of the samples versus the NaOH concentration. Other treatment conditions: 333 K and 2 h. The horizontal dotted lines represent the S_{meso} and V_{micro} of the parent ferrierite.

than the Al concentration, confirming the selective leaching of silicon in ferrierite. The yield of the treatment, defined as grams of solid after alkaline workup per gram of parent zeolite, decreased with an increased amount of leached silicon and ranged from 40 to 85 wt.% (Table 2). Although representative, the yield might be somewhat underestimated (by ca. 10%) owing to unavoidable solid losses during filtration of the treated dispersion and the relatively small amount of sample used in desilication experiments (166 mg).

3.2.3. Structure

The X-ray diffractograms in Fig. 2 show that the long-range crystallinity of the parent ferrierite is preserved in the alkaline-treated samples, despite the above-described changes in porosity. One of the few exceptions is AT-13 (V_{micro} = 0.01 cm^3 g^{-1}), which presents a silent diffraction pattern. In this case, the zeolite transformed into an amorphous material due to the severe desilication conditions applied (1 M NaOH, 353 K, 3 h).

The parent and treated zeolites were also characterized by nuclear magnetic resonance spectroscopy in order to investigate the location and chemical surrounding of silicon and aluminum. The ^{27}Al MAS-NMR spectrum of the parent ferrierite shows the characteristic peak at 54 ppm (Fig. 7a) due to tetrahedrally coordinated aluminum in the ferrierite lattice [5,8,13]. No peak at −2 ppm, typically assigned to extra-framework Al atoms in octahedral coordination, was discerned. The mesoporous ferrierites have practically identical spectra, suggesting that the aluminum coordination was not altered by the alkaline treatment. The ^{29}Si MAS-NMR spectra of ferrierite are typically composed of five peaks assigned to different tetrahedral sites in the unit cell [14,52]. The signals are often grouped in two types denoted T_A and T_B, which make reference to non-equivalent lattice positions. As expected, deconvolution of the ^{29}Si spectrum of the parent zeolite led to five contributions (Fig. 7b) centered at −104 ppm (SiOH), −106.5 ppm (Si(1Al) T_A), −110.5 ppm (Si(1Al) T_B), −113.5 ppm (Si(0Al) T_B), and −117.5 ppm (Si(0Al) T_A). Upon alkaline treatment, the ratio of the Si(0Al) and Si(1Al) contributions decreased due to the preferential leaching of silicon which is not surrounded by aluminum. This can be expected, as the negatively charged AlO_4^- tetrahedra prevent the hydrolysis of the Si–O–Al bond in the presence of OH^- in comparison with the relatively easy cleavage of the Si–O–Si bond in the absence of neighboring Al [35,43]. Other noticeable changes in the ^{29}Si spectra are (i) the growth and widening of the band at −104 ppm, indicating a higher exposure of surface silanol groups in the alkaline-treated ferrierite samples and (ii) the decreased area ratio of the bands at −117.5 and −113.5 ppm, suggesting a more favorable desilication of the Si(0Al) T_A sites. The latter two peaks are not discernable in AT-11 due to the harsh desilication conditions that seem to affect the local structure of silicon.

3.2.4. Morphology

Morphological changes in the alkaline-treated ferrierite samples were studied by scanning and transmission electron microscopies. SEM of one of the optimal samples (AT-16) at different

Table 2
Chemical composition of alkaline-treated ferrierite samples and the resulting filtrates.

Sample	$(Si/Al)_{solid}$ (mol mol^{-1})	$(Si/Al)_{filtrate}$ (mol mol^{-1})	$[Si]_{filtrate}$ (mg l^{-1})	$[Al]_{filtrate}$ (mg l^{-1})	S_{meso}[a] (m^2 g^{-1})	Yield[b] (%)
P	29	–	–	–	28	–
AT-9	22	339	3340	9	49	78
AT-11	12	394	9802	24	107	42
AT-14	25	139	2181	15	22	85
AT-15	20	672	4793	7	70	70
AT-16	17	307	6481	20	93	48

[a] Mesopore surface area determined from N_2 adsorption.
[b] Grams of solid after alkaline treatment per gram of parent zeolite.

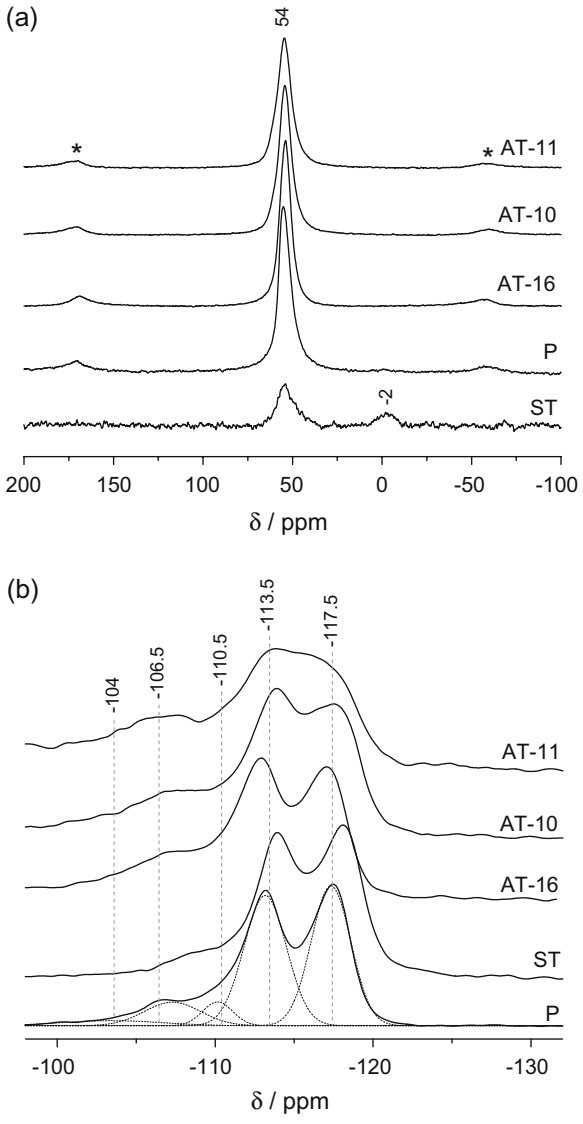

Fig. 7. (a) ^{27}Al and (b) ^{29}Si MAS-NMR spectra of the parent, steamed, and alkaline-treated ferrierite samples. Spinning side bands marked by asterisk.

magnifications (Fig. 3) reveals that NaOH induces (i) an impressive size decrease of the aggregated particles (compare micrographs a and c) and (ii) distinct dissolution of the platelets (compare micrographs b and d). TEM also substantiates crystal deaggregation and dissolution. The external surface of AT-16 (Fig. 4c) roughens significantly with respect to the parent sample (Fig. 4a) due to the attack of the crystals' external surface by the base. Besides, the formation of fissures at the edge of the crystals was occasionally detected (see arrows in Fig. 4d), although these were not frequently observed in this sample. AT-11 is visibly more damaged than AT-16 due to the harsher desilication conditions. The ferrierite platelets in AT-11 are ill defined and evidence the formation of holes, which mostly seem perpendicular to the crystal planes (Fig. 4e and f). This substantiates the ca. 45% reduction of V_{micro} in this sample with respect to the parent zeolite determined by N_2 adsorption.

The previous studies over ZSM-5 [35,36], ZSM-12 [37], mordenite [38], and beta [39,40] zeolites revealed the predominant generation of intracrystalline mesoporosity upon NaOH treatment due to silicon dissolution from the surface to the core of the crystals. However, SEM and TEM observations support that the mesoporosity introduced in alkaline-treated ferrierite has both inter- and intracrystalline components. Several mesoporosity-inducing processes seem to be involved, including deaggregation, exfoliation, fissuration, and perforation. Their relative importance depends on the desilication conditions, i.e. time, temperature, and NaOH concentration. Deaggregation and exfoliation already occur at milder treatment conditions and comprise the silicon hydrolysis leading to the separation of the agglomerated platy particles in ferrierite into smaller aggregates and thinner platelets. These mechanisms cause roughening of the external surface of the crystals and lead to intercrystalline mesoporosity, while the micropore volume is not penalized significantly (AT-15 and AT-16). Harsher treatments (e.g. AT-11) enable NaOH to make cracks or fissures and to perforate the ferrierite platelets, generating intracrystalline porosity. The latter processes sensibly affect the zeolite microporous properties.

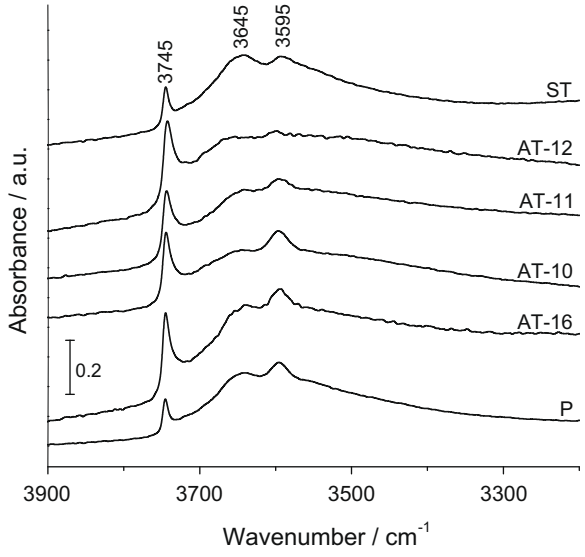

Fig. 8. FTIR spectra in the OH-stretching region of the parent and treated ferrierite samples.

3.2.5. Acidity

The acidity of the ferrierite samples was studied by FTIR and NH_3-TPD. Prior to the characterization, the NaOH-treated zeolites were converted into the protonic form by ion exchange in ammonium nitrate followed by calcination (see Section 2.1). Fig. 8 shows infrared spectra of selected samples in the OH-stretching region. The parent zeolite displays the characteristic bands at 3745 cm^{-1} due to isolated silanol groups and at 3595 cm^{-1} due to framework Al–OH (Brønsted acid sites) [53]. In addition, a broad band at 3645 cm^{-1} assigned to OH groups connected to extra-framework aluminum species, EF_{Al} (Lewis acid sites) [54], is discerned. The appearance of the latter feature contrasts with the ^{27}Al MAS-NMR spectra of the parent ferrierite, which did not show the characteristic peak of EF_{Al} around 0 ppm (Fig. 7a). Accordingly, it seems that the starting material contains some extra-framework Al although these species were not detected by nuclear magnetic resonance. Aluminum in highly distorted coordination might become NMR silent, and this has been referred to as 'invisible' aluminum [14,55]. It has been reported that quantitative determination of aluminum by ^{27}Al MAS-NMR can be attained by the use of fully hydrated samples and very short radiofrequency pulses [56].

Upon alkaline treatment, all the samples developed isolated silanol groups as revealed by the increased intensity of the band at 3745 cm^{-1}. This change, consistent with ^{29}Si MAS-NMR results, is due to the enhanced external surface in the desilicated zeolites due to mesopore development [35,40,41]. The intensity of the band at 3595 cm^{-1} in the optimal AT-16 sample is very similar to that in P, strongly suggesting the preserved Brønsted acidity in the mesoporous zeolite. This conclusion is further supported by temperature-programmed desorption of ammonia. The NH_3-TPD profiles of P and AT-16 in Fig. 9 resemble substantially, displaying a main broad peak centered at 740 K, which is assigned to strong (Brønsted) acid sites, and a small peak at 530 K attributed to weak (Lewis) acid sites [8,57]. The NH_3 uptake in P was 0.46 mmol g^{-1} and increased to 0.63 mmol g^{-1} in AT-16 as a consequence of the lower Si/Al ratio in the alkaline-treated zeolite (see Table 2).

The samples AT-10, AT-11, and AT-12 were treated at increasing NaOH concentration, i.e. 0.35, 0.5, and 0.75 M, respectively (see Table 1 and Fig. 6). The decrease of the band at 3595 cm^{-1} in the OH-stretching region of the infrared spectra (Fig. 8) is due to the progressive depletion of Brønsted acidity caused by a more severe alkaline treatment. In good agreement with infrared as well as ^{27}Al MAS-NMR characterizations, the uptake of ammonia by AT-11 (Fig. 9) and AT-12 (not shown) was lowered in the high-temperature region (750 K) and a broad contribution in the low-temperature region (600 K) is more prominent due to the significant damage of the microporous structure. In infrared, the intensity of the absorption at 3645 cm^{-1}, assigned to extra-framework aluminum, was similar in the parent and optimal alkaline-treated (AT-16) samples. However, this band decreases in the samples treated under harsh conditions, i.e. AT-10, AT-11, and AT-12. It could be that severe treatment conditions favor leaching of extra-framework aluminum. In support to this, the aluminum content in the filtrate of the AT-11 sample is somewhat higher (Table 2). However, this is a tentative interpretation as spectral changes in DRIFTS cannot be quantified.

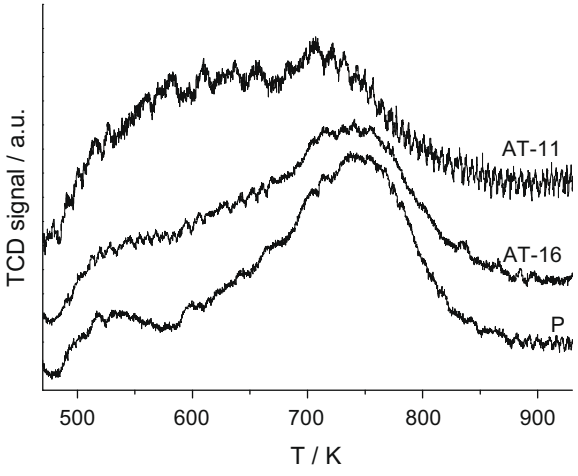

Fig. 9. NH_3-TPD profiles of the parent ferrierite and alkaline-treated ferrierite samples.

3.3. Desilication versus dealumination

For comparative purposes, the parent zeolite was subjected to steam (ST) or acid leaching (HCl) post-treatments. In contrast to desilication, dealumination did not modify the porosity of ferrierite (Table 1). The inability of dealumination treatments to introduce porosity in ferrierite with lower Si/Al ratios than that used in this work has been reported elsewhere [5,8,13,32,33,58]. However, changes in the structure and acidic properties of the zeolite were provoked due to framework Al extraction. This is concluded from ^{27}Al MAS-NMR (Fig. 7). The spectrum of ST shows a strong decrease of intensity and broadening of the peak at 54 ppm due to tetrahedrally coordinated aluminum and the appearance of a −2 ppm due to octadehedrally coordinated aluminum in extra-framework positions. Besides, the intensity of the resonance at −105 ppm due to Si(1Al) in the ^{29}Si NMR spectra decreased. In connection with dealumination, the intensity of the infrared absorption at 3595 cm^{-1} associated with Brønsted acid sites decreased in the steamed and acid-leached samples (Fig. 8). Concomitantly, the broad band centered at 3645 cm^{-1} increased due to the formation of EF_{Al}.

Finally, we addressed whether the presence of extra-framework Al species in the parent ferrierite, as hinted by the infrared band at 3645 cm^{-1}, has any influence on the amount of mesoporosity developed by desilication. It is known that EF_{Al} generated by steam treatment inhibits Si extraction and related mesopore formation in ZSM-5 [35,59]. This was attributed to re-alumination of the extra-framework Al species during the alkaline treatment. The blockage of zeolite micropores by EF_{Al} might also contribute to the lower amount of mesopores formed. Accordingly, the steam-treated ferrierite (ST) was subjected to one of the optimal alkaline-treatment conditions (0.2 M, 363 K, 3 h), leading to ST-AT-15 (Table 1). In agreement with the previous results over ZSM-5, the mesopore surface area of ST-AT-15 (50 $m^2\ g^{-1}$) is lower than that of AT-15 (70 $m^2\ g^{-1}$). Attending to this result, one could speculate that NaOH treatment (e.g. at the conditions of AT-15) of EF_{Al}-free ferrierite may eventually lead to a somewhat higher S_{meso} than 70 $m^2\ g^{-1}$. We treated the parent ferrierite in oxalic acid (OA) in order to wash EF_{Al} species and subjected the resulting solid to NaOH treatment (OA-AT-15). However, the applied oxalic acid treatment neither changed the textural properties of the parent zeolite (OA in Table 1) nor removed the infrared band at 3645 cm^{-1} (not shown). In support to these observations, it has been reported that oxalic acid [32] and even hydrochloric acid [13] do not remove EF_{Al} in ferrierite as no variation in the bulk Si/Al ratio can be seen after the different treatments. Accordingly, the porous properties of OA-AT-15 and AT-15 are practically identical.

3.4. LDPE pyrolysis

The generation of mesoporosity and structural defects upon optimal NaOH treatment coupled with the preservation of intrinsic zeolite properties may have a positive influence on the catalytic performance of ferrierite due to improved active site accessibility.

The acid-catalyzed degradation of low-density polyethylene was chosen to investigate whether the textural changes generated are ultimately functional in catalysis. As stated at the end of the Introduction, this application is of practical importance for chemical recycling of plastic waste. The diameter of the branched polyethylene chain (0.494 nm [45]) exceeds the size of the 8-MR channels (0.35 × 0.48 nm) of FER, and is very similar to the size of the main 10-MR channels (0.42 × 0.54 nm). The strong diffusion limitations in ferrierite, caused by impeded access of the branched polymer into the zeolite micropore system, explain its poor pyrolysis performance in comparison with other zeolite matrices such as beta, mordenite, and Y [45]. However, the advantage of using small-pore zeolites (MFI, MWW, FER) is that they lead mostly to gaseous products (olefins) and have an excellent resistance to coke formation in contrast to large-pore zeolites (BEA, FAU) [60–64].

The catalytic activity of the ferrierite zeolites was evaluated by thermogravimetry, i.e. monitoring the weight loss upon applying a temperature ramp in nitrogen and keeping the polymer-to-zeolite mass ratio of 3. The profiles of LDPE conversion into volatile compounds versus temperature over selected samples are shown in Fig. 10. Effluent analysis was not conducted, as our prime goal was to prove whether the introduction of different degrees of mesoporosity lowers the degradation temperature of the polymer with respect to the purely microporous zeolite. The thermal LDPE pyrolysis (indicated by dashed line) was shifted by ca. 40 K to lower temperature in the presence of the parent ferrierite (indicated by open circles). Agullo et al. [45] reported a decrease of ca. 80 K using a commercial H-ferrierite with Si/Al ratio of 10, i.e. having three times more aluminum than the parent ferrierite used in this work. The temperature for LDPE degradation was further decreased over the alkaline-treated ferrierite samples. The best catalyst was AT-16, in which a T_{50} (temperature for 50% conversion) of ca. 650 K was attained, i.e. 65 K lower than that in the parent ferrierite. The difference in T_{50} reported in [45] between the most (H-beta) and least active (H-ferrierite) zeolites having a similar Si/Al ratio was <50 K, giving an idea of the significant improvement upon optimal alkaline treatment of ferrierite. The enhanced pyrolysis activity of polyethylene over hierarchical ZSM-5 [65] and beta [40] zeolites prepared by desilication with respect to their corresponding purely microporous counterparts has been reported. As shown in Fig. 10, steam treatment is detrimental for the catalytic activity of ferrierite (indicated by solid triangles). This can be expected due to the depletion of active Brønsted acid sites by dealumination and the unaltered porous properties of the zeolite.

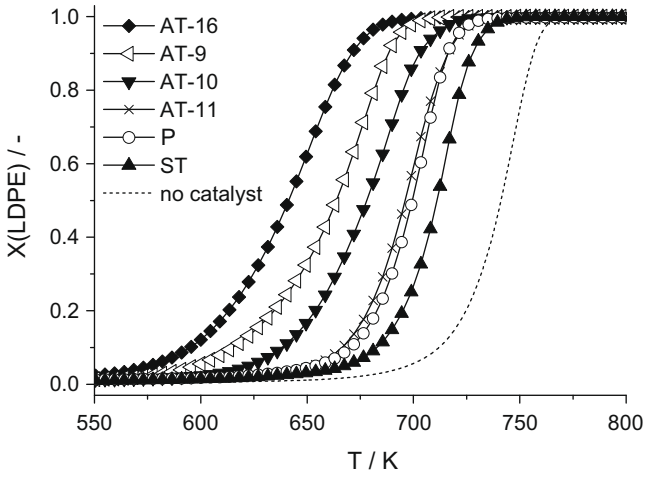

Fig. 10. LDPE conversion versus temperature during pyrolysis tests over the parent, steamed, and alkaline-treated ferrierite zeolites. Heating rate = 10 K min^{-1}.

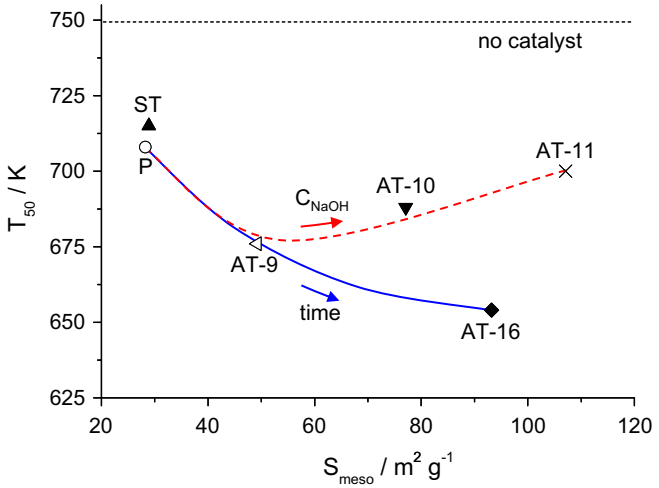

Fig. 11. Correlation between the catalytic activity (T_{50}) from the conversion profiles in Fig. 10 and the mesopore surface area of the samples.

A more detailed analysis of the LDPE conversion profiles is given in Fig. 11, which depicts the T_{50} versus the mesopore surface area of the samples. Two distinct behaviors are plotted to further illustrate that the desilication treatment for mesoporosity generation should be carefully optimized in relation to the particular catalytic application. The series of samples P, AT-9, and AT-16 shows a clear correlation between the catalytic activity and the mesopore surface area (indicated by solid line). AT-9 and AT-16 were treated during 3 and 9 h, respectively, using the same NaOH concentration (0.2 M) and temperature (353 K). The improved pyrolysis performance over the hierarchical zeolites can be attributed to the increased external surface area and amount of exposed acid sites as a consequence of the secondary mesoporosity. LDPE cracking follows a similar chemistry to the cracking of smaller hydrocarbon molecules [66]. With these large molecules, diffusion limitations can be expected to play a significant role, which are alleviated by introducing mesoporosity due to shorter diffusion path lengths. Fig. 11 also illustrates that inducing excessive mesoporosity can be detrimental for the pyrolysis activity (indicated by dashed line) if the unique zeolite properties are seriously affected. The mesopore surface area of AT-9, AT-10, and AT-11 increased due to the application of progressively higher NaOH concentrations (see Fig. 6). However, the catalytic activity decreases due to the substantial loss of microporosity. The effect of the enhanced active site accessibility is counterbalanced by the loss of active sites. For example, the performance of AT-11 (S_{meso} = 107 m^2 g^{-1}, 43% loss of microporosity) approaches that of the parent ferrierite.

The molar Si/Al ratio in the hierarchical zeolites decreases upon increasing the degree of mesoporosity due to the larger fraction of silicon extracted (Table 2). More aluminum implies more acid centers per gram of zeolite, which could also contribute to the improved LDPE degradation performance of the modified zeolites. However, the better accessibility due to mesopore creation appears to be the dominating factor for explaining the activity differences. The LDPE conversion corrected by the aluminum content in each catalyst provides the same trend as in Fig. 10. For example, AT-9 and AT-16 are 4.5 and 6.5 times more active per Al atom compared to P, respectively, indicating that the turnover frequency is enhanced due to the more effective active site utilization.

Finally, we conducted a kinetic study using the Ozawa method (Eq. (1)) [49]. For this purpose, LDPE pyrolysis was conducted at different heating rates (β) ranging from 5 to 50 K min^{-1} as described in Section 2.3. Fig. 12 shows the non-isothermal Ozawa activation energy versus the degree of LDPE conversion in thermal

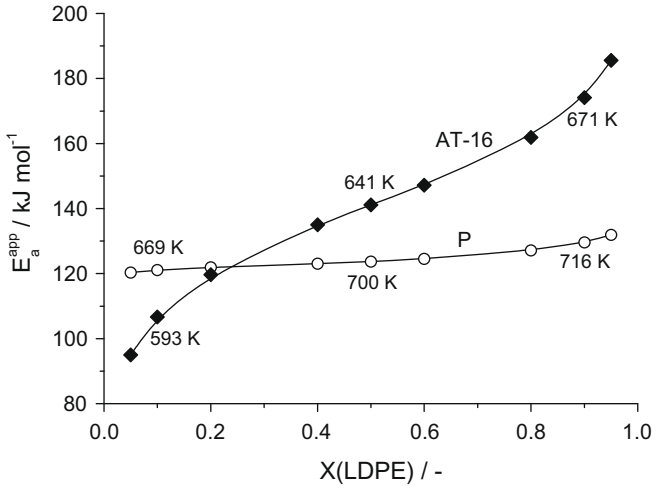

Fig. 12. Apparent activation energy determined by the Ozawa method [49] versus the LDPE conversion over the parent and alkaline-treated ferrierite zeolites.

and catalytic processes. The temperatures associated with 10%, 50%, and 90% conversion are indicated. The apparent activation energy of LDPE pyrolysis over the parent ferrierite was 120 kJ mol^{-1} and slightly increased with the degree of polymer conversion. In contrast, the alkaline-treated ferrierite showed a lower E_a^{app} at X(LDPE) < 10% (95 kJ mol^{-1}) and progressively increased with the degree of polymer conversion (up to 185 kJ mol^{-1}). According to Serrano et al. [61], LDPE degradation starts with the initial cracking followed by oligomerization, cyclization, and hydrogen transfer reactions that result in the formation of aromatics, light parafins, and olefins. The lower E_a^{app} over AT-16 at low degrees of LDPE conversion is tentatively attributed to the facilitated cracking of the long polyethylene chains into small C3–C5 olefins on the more accessible acid sites of the hierarchical ferrierite zeolite. The increasing activation energy over the mesoporous ferrierite strongly suggests that the role of mesopores in ferrierite is not limited to lower the degradation temperature of the polymer, but also induces important changes in the product distribution due to reduced diffusion constraints. Following the recent interpretations by Saha and Goshal [67] related to LDPE pyrolysis with ZSM-5, we put forward that the increasing E_a^{app} over AT-16 is due to the formation of aromatics through cyclization, while catalytic cracking of the high-molecular weight fragments to give liquid and/or gas occurs almost exclusively over the purely microporous ferrierite. Oligomerization and cyclization reactions are favored over the mesoporous zeolites due to the improved access. Consequently, inducing hierarchy in zeolites generates more active catalysts and in addition enables certain manipulation of the selectivity to products. The enhanced performance of mesoporous ferrierite highlights the improvement margin of known zeolites in heterogeneous catalysis. The use of mesoporous ferrierite is expected to have an impact on the various reactions cited in the Introduction. Some of them will be subject of upcoming investigations.

4. Conclusions

In contrast to dealumination treatments, desilication of commercial ferrierite in aqueous NaOH solution under optimal conditions leads to 3-4 times higher mesopore surface area with respect to the parent zeolite, while mostly preserving the native acidity and crystallinity. The attack by NaOH induces deaggregation, exfoliation, fracture, and ultimately perforation of the ferrierite crystals, resulting in mesoporosity of combined inter- and intracrystalline nature. Subtle optimization of the treatment conditions (temperature, time, and NaOH concentration) is required to introduce mesoporosity without significantly altering the micropore structure due to excessive Si leaching. Compared to other frameworks (MFI, MTW, MOR, and BEA), mesopore formation by desilication in FER requires harsher conditions likely due to the high stability of framework Al in ferrierite. The stability of framework Al is vital for directing silicon leaching toward mesopore formation. Furthermore, desilication of FER does not lead to defined mesopore size distributions, which has been related to the characteristic crystal morphology consisting of thin platelets. The introduction of mesoporosity in the hierarchical zeolites enhanced the LDPE degradation performance with respect to the parent zeolite (purely microporous), and appears to alter the product distribution. The latter requires verification by analysis of reaction products. In any case, these effects are largely a consequence of the improved accessibility of the polymer molecules to the active sites, due to increased external surface area, shorter diffusion path lengths, and the presence of defects in the modified zeolites. However, the formation of mesopores was ineffectual for catalysis if the treatment involves serious damage of the intrinsic crystallinity and acidity.

Acknowledgments

This research was funded by the Spanish MICINN (Project CTQ2006-01562/PPQ and Consolider-Ingenio 2010 Grant CSD2006-0003) and the ICIQ Foundation.

References

[1] S. Ernst, Angew. Chem. Int. Ed. 35 (1996) 63.
[2] A. Corma, Chem. Rev. 97 (1997) 2373.
[3] M. Hartmann, Angew. Chem. Int. Ed. 43 (2004) 5880.
[4] J. Pérez-Ramírez, C.H. Christensen, K. Egeblad, C.H. Christensen, J.C. Groen, Chem. Soc. Rev. 37 (2008) 2530.
[5] R.J. Pellet, D.G. Casey, H.-M. Huang, R.V. Kessler, E.J. Kuhlman, C.-L. O'Young, R.A. Sawicki, J.R. Ugolini, J. Catal. 157 (1995) 423.
[6] F.C. Meunier, L. Domokos, K. Seshan, J.A. Lercher, J. Catal. 211 (2002) 366.
[7] K. Föttinger, G. Kinger, H. Vinek, Appl. Catal. A 249 (2003) 205.
[8] D.P.B. Peixoto, S.M. Cabral de Menezes, M.I. Pais da Silva, Mater. Lett. 57 (2003) 3933.
[9] C.L. Kibby, A.J. Perrotta, F.E. Massoth, J. Catal. 35 (1974) 256.
[10] B.G. Anderson, R.R. Schumacher, R. van Duren, A.P. Singh, R.A. van Santen, J. Mol. Catal. A: Chem. 181 (2002) 291.
[11] B.R. Cook, J.W. Johnson, G. Cao, R.A. McEvoy, US Patent 6013171, 2000.
[12] C. Jimenez, F.J. Romero, R. Roldan, J.M. Marinas, J.P. Gomez, Appl. Catal. A 249 (2003) 175.
[13] R. Rachwalik, Z. Olejniczak, B. Sulikowski, Catal. Today 101 (2005) 147.
[14] R. Rachwalik, Z. Olejniczak, J. Jiao, J. Huang, M. Hunger, B. Sulikowski, J. Catal. 252 (2007) 161.
[15] D. Kaucky, F. Fajula, P. Moreau, A. Finiels, Appl. Catal. A 243 (2003) 301.
[16] J.W. Yoon, J.H. Lee, J.-S. Chang, D.H. Choo, S.J. Lee, S.H. Jhung, Catal. Commun. 8 (2007) 967.
[17] M.A. Aramendia, V. Borau, C. Jimenez, J.M. Marinas, R. Roldan, F.J. Romero, F.J. Urbano, Chem. Lett. (2002) 672.
[18] R. Anand, S.S. Shevade, R.K. Ahedi, S.P. Mirajkar, B.S. Rao, Catal. Lett. 62 (1999) 209.
[19] R. Bulanek, K. Novoveska, B. Wichterlova, Appl. Catal. A 235 (2002) 181.
[20] B. Sulikowski, J. Janas, J. Haber, A. Kubacka, Z. Olejniczak, E. Włoch, Chem. Commun. (1998) 2755.
[21] M. Petersson, T. Holma, B. Andersson, E. Jobson, A. Palmqvist, J. Catal. 235 (2005) 114.
[22] A. Guzman-Vargas, G. Delahay, B. Coq, Appl. Catal. B 42 (2003) 369.
[23] P.A. Vaughan, Acta Crystallogr. 21 (1966) 983.
[24] Ch. Baerlocher, L.B. McCusker, D.H. Olson, Atlas of Zeolite Framework Types, sixth ed., Elsevier, Amsterdam, 2007.
[25] E. Włoch, A. Łukaszczyk, Z. Żurek, B. Sulikowski, Catal. Today 114 (2006) 231.
[26] W.J.M. van Well, X. Cottin, J.W. de Haan, R.A. van Santen, B. Smit, Angew. Chem. Int. Ed. 37 (1998) 1081.
[27] A. Corma, V. Fornes, S.B. Pergher, T.L.M. Maesen, J.G. Buglass, Nature 396 (1998) 353.
[28] L. Tosheva, V.P. Valtchev, Chem. Mater. 17 (2005) 2494.
[29] J. Čejka, S. Mintova, Catal. Rev. -Sci. Eng. 49 (2007) 457.
[30] K. Egeblad, C.H. Christensen, M. Kustova, C.H. Christensen, Chem. Mater. 20 (2008) 946.
[31] A. Corma, U. Diaz, M.E. Domine, V. Fornés, J. Am. Chem. Soc. 122 (2000) 2804.
[32] M. Müller, G. Harvey, R. Prins, Micropor. Mesopor. Mater. 34 (2000) 135.

[33] G. Onyestyák, J. Valyon, G. Pál-Borbély, L.V.C. Rees, Appl. Surf. Sci. 196 (2002) 401.
[34] S. van Donk, A.H. Janssen, J.H. Bitter, K.P. de Jong, Catal. Rev. -Sci. Eng. 45 (2003) 297.
[35] J.C. Groen, L.A.A. Peffer, J.A. Moulijn, J. Pérez-Ramírez, Chem. Eur. J. 11 (2005) 4983.
[36] J.C. Groen, J.A. Moulijn, J. Pérez-Ramírez, J. Mater. Chem. 16 (2006) 2121.
[37] X. Wei, P.G. Smirniotis, Micropor. Mesopor. Mater. 97 (2006) 97.
[38] J.C. Groen, T. Sano, J.A. Moulijn, J. Pérez-Ramírez, J. Catal. 251 (2007) 21.
[39] J.C. Groen, S. Abelló, L.A. Villaescusa, J. Pérez-Ramírez, Micropor. Mesopor. Mater. 114 (2008) 93.
[40] J. Pérez-Ramírez, S. Abelló, A. Bonilla, J.C. Groen, Adv. Funct. Mater. 19 (2009) 164.
[41] J. Pérez-Ramírez, S. Abelló, L.A. Villaescusa, A. Bonilla, Angew. Chem. Int. Ed. 47 (2008) 7913.
[42] J.C. Groen, L.A.A. Peffer, J.A. Moulijn, J. Pérez-Ramírez, Micropor. Mesopor. Mater. 69 (2004) 29.
[43] J.C. Groen, J.C. Jansen, J.A. Moulijn, J. Pérez-Ramírez, J. Phys. Chem. B 108 (2004) 13062.
[44] J. Aguado, D.P. Serrano, Feedstock Recycling of Plastic Wastes, The Royal Society of Chemistry, Cambridge, 1999.
[45] J. Agullo, N. Kumar, D. Berenguer, D. Kubicka, A. Marcilla, A. Gómez, T. Salmi, D.Y. Murzin, Kinet. Catal. 48 (2007) 535.
[46] S. Brunauer, P.H. Emmett, E. Teller, J. Am. Chem. Soc. 60 (1938) 309.
[47] B.C. Lippens, J.H. de Boer, J. Catal. 4 (1965) 319.
[48] E.P. Barrett, L.G. Joyner, P.P. Halenda, J. Am. Chem. Soc. 73 (1951) 373.
[49] T. Ozawa, Bull. Chem. Soc. Jpn. 38 (1965) 1881.
[50] M. Ogura, S.Y. Shinomiya, J. Tateno, Y. Nara, M. Nomura, E. Kikuchi, H. Matsukata, Appl. Catal. A 219 (2001) 33.
[51] J.C. Groen, L.A.A. Peffer, J.A. Moulijn, J. Perez-Ramírez, Colloids Surf. A 241 (2004) 53.
[52] P. Sarv, B. Wichterlová, J. Čejka, J. Phys. Chem. B 102 (1998) 1372.
[53] A. Zecchina, S. Bordiga, G. Spoto, D. Scarano, G. Petrini, G. Leofanti, M. Padovan, J. Chem. Soc. Faraday Trans. 88 (1992) 2959.
[54] I. Kiricsi, C. Flego, G. Pazzuconi, W.O. Parker, R. Millini, C. Perego, G. Bellussi, J. Phys. Chem. 98 (1994) 4627.
[55] P.P. Man, J. Klinowski, Chem. Phys. Lett. 147 (1988) 581.
[56] P.P. Man, J. Klinowski, J. Chem. Soc. Chem. Commun. (1988) 1291.
[57] B.S. Kwak, J. Sung, Catal. Lett. 53 (1998) 125.
[58] W.-Q. Xu, Y.-G. Yin, S.L. Suib, J.C. Edwards, C.-L. O'Young, J. Catal. 163 (1996) 232.
[59] J.C. Groen, J.A. Moulijn, J. Pérez-Ramírez, Micropor. Mesopor. Mater. 87 (2005) 153.
[60] J.W. Park, J.-H. Kim, G. Seo, Polym. Degrad. Stab. 76 (2002) 495.
[61] D.P. Serrano, J. Aguado, J.M. Escola, Ind. Eng. Chem. Res. 39 (2000) 1177.
[62] K. Gobin, G. Manos, Polym. Degrad. Stab. 86 (2004) 225.
[63] R.A. García, D.P. Serrano, D. Otero, J. Anal. Appl. Pyrol. 74 (2005) 379.
[64] H.J. Park, Y.-K. Park, J.-I. Dong, J.-K. Jeon, J.-H. Yim, K.-E. Jeong, Res. Chem. Intermed. 34 (2008) 727.
[65] D.H. Choi, J.W. Park, J.-H. Kim, Y. Sugi, Polym. Degrad. Stab. 91 (2006) 2860.
[66] D.P. Serrano, J. Aguado, J.M. Escola, J.M. Rodríguez, J. Anal. Appl. Pyrol. 74 (2005) 353.
[67] B. Saha, A.K. Ghoshal, Thermochim. Acta 453 (2007) 120.